The Astronomical Journal, 165:1 (6pp), 2023 January https://doi.org/10.3847/1538-3881/ac9eb8

Radio-loud Exoplanet-exomoon Survey: GMRT Search for Electron Cyclotron Maser Emission

Mayank Narang[1,7], Apurva V. Oza[2,3], Kaustubh Hakim[4], P. Manoj[1], Ravinder K. Banyal[5], and Daniel P. Thorngren[6]
[1] Tata Institute of Fundamental Research, Mumbai, India
[2] Jet Propulsion Laboratory, California Institute of Technology, Pasadena, USA
[3] Physikalisches Institut, Universität Bern, Bern, Switzerland
[4] University of Bern, Center for Space and Habitability, Bern, Switzerland
[5] Indian Institute of Astrophysics, Bangalore, India
[6] Université de Montréal, Quebec, Canada
[7] Academia Sinica Institute of Astronomy & Astrophysics, 11F of Astro-Math Bldg., No. 1, Sec. 4, Roosevelt Road, Taipei 10617, Taiwan, Republic of China
Received 2021 October 29; revised 2022 October 17; accepted 2022 October 24; published 2022 December 2

Abstract

We conducted the first dedicated search for signatures of exoplanet–exomoon interactions using the Giant Metrewave Radio Telescope (GMRT) as part of the radio-loud exoplanet-exomoon survey. Due to stellar tidal heating, irradiation, and subsequent atmospheric escape, candidate "exo-Io" systems are expected to emit up to 10^6 times more plasma flux than the Jupiter-Io DC circuit. This can induce detectable radio emission from the exoplanet-exomoon system. We analyze three "exo-Io" candidate stars: WASP-49, HAT-P 12, and HD 189733. We perform 12 hr phase-curve observations of WASP-49b at 400 MHz during primary & secondary transit, as well as first & third quadratures achieving a 3σ upper limit of 0.18 mJy beam^{-1} averaged over four days. HAT-P 12 was observed with GMRT at 150 and 325 MHz. We further analyzed the archival data of HD 189733 at 325 MHz. No emission was detected from the three systems. However, we place strong upper limits on radio flux density. Given that most exo-Io candidates orbit hot Saturns, we encourage more multiwavelength searches (in particular low frequencies) to span the lower range of exoplanet B-field strengths constrained here.

Unified Astronomy Thesaurus concepts: Natural satellites (Extrasolar) (483); Radio continuum emission (1340); Exoplanets (498); Star-planet interactions (2177)

1. Introduction

Extrasolar satellites (exomoons) have so far eluded ongoing searches due to their small size. Several investigations have exploited transit timing variations leading to the possible identification of giant exomoons (Teachey & Kipping 2018; Heller et al. 2019; Kreidberg et al. 2019). Recently, high-resolution spectroscopy has revealed that evaporating exomoons may display alkali metals in hot Jupiter/Saturn atmosphere transit spectra due to their inevitable outgassing due to tidal heating and plasma-driven atmospheric sputtering (Oza et al. 2019; Gebek & Oza 2020). These exomoon candidates have been named "exo-Ios" due to their extremely large evaporation rates $\sim 10^{8\pm2}$ kg s^{-1} (0.2–20 lunar mass Gyr^{-1}) capable of catastrophic self erosion over the often unconstrained age of the star system.

One possible method of detecting these elusive exomoons is to search for signals of planet–moon interactions. In the solar system, the planet–moon interaction between Jupiter and Io leads to detectable radio emission. The Io-controlled decametric emission (Bigg 1964) is caused by the motion of Io through Jupiter's magnetic field lines. This motion leads to magnetic field oscillations known as Alfvén waves (Belcher 1987), which lead to the generation of electric fields parallel to the Jovian magnetic field line (Neubauer 1980; Crary 1997; Saur et al. 2004; Su 2009). As the electrons travel through magnetic field lines, they accelerate and gyrate, leading to radio emission powered by the electron cyclotron maser instability mechanism (ECMI; Wu & Lee 1979; Crary 1997). If a similar mechanism also operates in exomoon-exoplanet systems, then their emission might also be radio bright.

There have been several attempts at detecting star–planet interaction in the radio and UV domain (e.g., Lazio et al. 2004; Smith et al. 2009; Lecavelier Des Etangs et al. 2011; Lecavelier des Etangs, et al. 2013; Hallinan et al. 2013; Vedantham et al. 2020; Callingham et al. 2021; Narang et al. 2021a, 2021b; Pérez-Torres et al. 2021; Turner et al. 2021; Viswanath et al. 2020). However, the exoplanet–exomoon interaction has not yet been studied observationally. In this work, we present the first dedicated survey for studying the planet–moon interaction using the Giant Metrewave Radio Telescope (GMRT) to reveal hidden volcanic exo-Ios (or their exotori counterparts) as well as inform the unknown field strengths of hot Jupiters and hot Saturns. In Section 2, we describe the targets, followed by the details of the observations and the data reduction process in Section 3. We describe the results in Section 4. In Section 5, we discuss our findings, followed by a summary in Section 6.

2. Targets

To select a sample of possible exomoon candidates, we consider planets with alkali exosphere detections in high-resolution spectroscopy (Wyttenbach et al. 2015, 2017; Dwivedi et al. 2019). The main target of our proposal is WASP-49. The WASP-49 system has never been observed at radio wavelengths. We also retrieve archival GMRT observations of two more exomoon candidates, HD 189733 and HAT-P 12. All three systems are candidate exo-Io systems based on the minimum sodium and potassium column densities implied

Table 1
Stellar and Planetary Parameters of the Systems Examined in this Work

Host star	Sp Ty	M_P	R_P	a_P	d	Reference
		(M_J)	(R_J)	(au)	(pc)	
WASP 49	G6 V	0.378 ± 0.027	1.115 ± 0.047	0.0379 ± 0.001	$193.73^{0.68}_{-0.52}$	Lendl et al. 2012
HAT-P 12	K4 V	0.21 ± 0.01	$0.959^{0.029}_{-0.021}$	0.0384 ± 0.0003	141.75 ± 0.18	Hartman et al. 2009
HD 189733	K2 V	1.166 ± 0.05	$1.142^{0.036}_{-0.034}$	0.031 ± 0.004	$19.76^{0.006}_{-0.005}$	Addison et al. 2019

Note. The distance d is from Gaia EDR3/DR3 Bailer-Jones et al. (2021).

by high-resolution visible light spectroscopy observations (Oza et al. 2019). These potentially evaporating exomoons are well within the tidal stability criterion (Cassidy et al. 2009). Evaporative transmission spectroscopy simulations of two of these systems (WASP-49, HD 189733) demonstrate that an exo-Io or exo-torus scenario is consistent with high-resolution sodium observations at present (Gebek & Oza 2020). In Table 1, we list the stellar and planetary parameters for WASP-49, HD 189733, and HAT-P 12 systems.

The system HD 189733 has been previously observed with GMRT at 150 MHz, 244 MHz, and 614 MHz (Lecavelier Des Etangs et al. 2009, 2011). At 150 MHz Lecavelier Des Etangs et al. (2011) obtained a $3\sigma$of 2.1 mJy beam^{-1} , while at 244 MHz and 614 MHz Lecavelier Des Etangs et al. (2009) derived a 3σ upper limit of 2 mJy beam^{-1} and 160 μJy beam^{-1} respectively. Smith et al. (2009) observed HD 189733 between 304 and 347 MHz with the Robert C. Byrd Green Bank Telescope of the National Radio Astronomy Observatory. The reached and rms sensitivity of 26.7 mJy beam^{-1}. No radio observations of HAT-P 12 have been carried out previously.

3. Observations and Data Reduction

It is unlikely to know a priori the orbital period of exomoons around their parent planets. Moreover, the radio beam, due to planet–moon interaction, may be arbitrarily oriented with respect to the observer. Furthermore, the emission can also be modulated based on the phase of the planet around the star as argued by Pérez-Torres et al. (2021). To maximize the likelihood of detecting the emission, we decided to observe the WASP-49 system at four phases of the planets around the star: the first and second quadrature of the planet WASP-49b, as well as the primary and secondary transit. The WASP-49b system was observed for 12 hr (spread over four observations) with uGMRT in band 3 (250–500 MHz, proposal ID 39_015). The center frequency of the receiver was set at 400 MHz, with a bandwidth of 200 MHz. For each observation, the phase center was set at the position of WASP-49b.

The primary transit of WASP-49b was observed on 2020 October 29. We observed 3C48 as the primary flux density and bandpass calibrator. The flux calibrator was observed twice, once at the beginning of the observation and once at the end of the observation. The phase calibrator used was $0521 - 207$ and was observed in a loop with 30 minutes on the science target and 5 minutes on $0521 - 207$. The secondary transit was observed on 2020 November 5, while the first quadrature (phase 0.25) was observed on 2020 November 8. The observational setup for these observations was similar to the night of 2020, October 29th, with 3C48 as the primary flux density and bandpass calibrator and $0521 - 207$ as the phase calibrator. The second quadrature (phase 0.75) was observed on 2021, January 17th. We used 3C147 as the primary flux density and bandpass calibrator, which was observed at the beginning as well as the end of the observation. We used 0706-231 as the phase calibrator, which was again observed in a loop of 5 minutes on the phase calibrator and 30 minutes on WASP-49.

We reduce the uGMRT data using the CASA Pipeline-cum-Toolkit for Upgraded Giant Metrewave Radio Telescope data REduction uGMRT- (CAPTURE) pipeline (Kale & Ishwara-Chandra 2021). We carry out the primary beam correction to correct for the falling sensitivity at the beam edges using the CASA task *wbpbgmrt*[8] to produce the final image.

We further analyze archival GMRT observations of the exoplanet systems HAT-P 12 and HD 189733. The HAT-P 12 field was observed at 150 MHz and 325 MHz with GMRT. At 150 MHz, the system was observed for 11.6 hr (proposal ID 20).

textsubscript089) on 2011, April 28th. The phase center of the observation was the HAT-P 12 system. 3C48 was used as the primary flux density, and $1331 + 305$ was used as the phase calibrator. At 325 MHz, the HAT-P 12 field was observed surreptitiously as part of the proposal 22.

textsubscript051 on 2012 September 8th. The phase center was set to the $J1357 + 43$, which is $24\farcm4$ away from HAT-P 12. The system was observed for $\sim$7 hr, with 3C286 being used as the flux calibrator and $1331 + 305$ as the phase calibrator.

We also retrieve previously unpublished uGMRT observations of the system HD 189,733 at 325 MHz. The system was observed for 9.3 hr on 2009 May 26, with the phase center being HD 189733. The primary flux calibrators used were 3C147 and 3C286, while $1924 + 334$ was used as the phase calibrator. The archival GMRT observations of HAT-P 12 and HD 189733 were reduced using the Source Peeling and Atmospheric Modeling pipeline (Intema 2014). The log of the observations is given in Table 2.

4. Results

The WASP-49 field was observed with the uGMRT at 400 MHz for four nights totaling 12 hr of observation time. The four observations for the WASP-49 field at 400 MHz are shown in Figure 1. No emission was detected for each of the observations. The rms values achieved for each of the four nights are listed in Table 2. Based on these rms values, we put a 3σ upper limit of 0.18 mJy beam^{-1} for the emission from this system.

In Figure 2, we show the archival GMRT observations for the HAT-P 12 system. At 150 MHz, we reached an rms value of 530 μJy beam^{-1}, and at 325 MHz, we were able to reach an rms value of 95 μJy beam^{-1}. No radio emission was, however, detected from the system at either of the frequencies. The upper limits of 1.6 mJy beam^{-1} at 150 MHz is comparable to some of

[8] https://github.com/ruta-k/uGMRTprimarybeam

Table 2
The Observation log and rms Sensitivity Achieved in this Work and in Literature

Target	Frequency	Phase	Date of Observation	Bandpass & Flux Density Calibrator	Phase Calibrator	rms this Work	rms Literature
	(MHz)	...	...	...	...	(μJy beam^{-1})	(μJy beam^{-1})
WASP 49b[2]	400	Primary transit	2020 October 30th	3C48	0521 − 207	79	...
WASP 49b[2]	400	First quadrature	2021 January 18th	3C147	0706 − 231	78	...
WASP 49b[2]	400	Secondary eclipse	2020 November 5th	3C48	0521 − 207	72	...
WASP 49b[2]	400	Second quadrature	2020 November 8th	3C48	0521 − 207	61	...
HAT-P 12b	150	...	2011 April 28th	3C48	1331 + 305	530	...
HAT-P 12b	325	...	2012 September 8th	3C286	1331 + 305	95	...
HD 189733b	325	...	2009 May 26th	3C147 & 3C286	1924 + 334	118	26,667[a]

Note.
[2] P.I: A. Oza ID39_015; a Smith et al. (2009).

the deepest limits reached at that frequency for an exoplanet field (e.g., Hallinan et al. 2013; O'Gorman et al. 2018; Narang et al. 2021b; Narang 2022). The GMRT observations of HD 189,733 325 MHz are shown in Figure 3. At 325 MHz, the rms value for the HD 189733 field is 95 μJy beam^{-1}.

5. Discussion

During our observations, we have produced some of the deepest images of an exoplanet field (e.g., Lecavelier Des Etangs et al. 2011; Lecavelier des Etangs, et al. 2013; Hallinan et al. 2013; O'Gorman et al. 2018; Narang et al. 2021b; Pérez-Torres et al. 2021; Narang 2022). There could be several reasons why no radio emission was detected from these systems. In the following subsection, we discuss some of these possible reasons.

5.1. Radio-quiet Exoplanet-exomoon Emission

If the radio emission from exoplanet-exomoon interaction is inherently quiet, in that case, our current instrumentation will not be able to detect it. A major difficulty in our experiment is the sheer distance of the targets; for instance, 2/3 of the candidate exomoon targets we analyzed in this study are located beyond 100 pc; therefore, the flux emitted may be too weak to be detected with uGMRT. Moreover, deeper observations with next-generation radio telescopes are needed to detect radio-quiet exoplanet-exomoon emissions.

5.2. Overestimation of Cyclotron Frequency and Exoplanet Magnetic Fields

The electron cyclotron maser emission is characterized by the maximum cyclotron emission frequency ν_c. This frequency for ECMI masers is fundamentally linked to the magnetic field strength B_0 of the emitting body at the radio source location and is given as follows:

$$\nu_c = 2.8 B_0 \tag{1}$$

where B_0 is in Gauss and ν_c in MHz.

The observations in this work have been carried out at frequencies in the range of 150–500 MHz. This corresponds to planetary magnetic fields of ∼50–180 G. If the magnetic fields of the exoplanets are lower than these values, then we could have missed the emission.

To evaluate this possibility, we apply the methods of Yadav & Thorngren (2017) to estimate the magnetic fields using evolution modeling (Thorngren & Fortney 2018) to derive the heat flux from the interiors of the planets (see Christensen et al. 2009). This gives the mean magnetic field on the dynamo surface as (from Reiners & Christensen 2010)

$$B_{\rm rms}^{\rm dyn}\ [\rm kG] = 4.8 \times 10^3 (M_P L_P^2)^{1/6} R_P^{-7/6}, \tag{2}$$

where M_P, L_P, and R_P are the mass, luminosity, and radius of the planet (all normalized to solar values).

However, the dynamo surface is not at the surface of the planet but further in at the liquid–metallic phase transition at approximately 1 Mbar (Yadav & Thorngren 2017; Chabrier et al. 2019). To best take this into account, we adapt Equation (2) of Yadav & Thorngren (2017), which uses a scaling law for the dynamo radius (which was calibrated for planets with $M_P \sim 1 M_J$, to instead use the 1 Mbar radius from our evolution models. The dipole magnetic field strength at the pole is thus

$$B_{\rm dipole}^{\rm polar} = \frac{B_{\rm rms}^{\rm dyn}}{\sqrt{2}} \left(\frac{R_{\rm dyn}}{R_P} \right)^3, \tag{3}$$

where $R_{\rm dyn}$ is the dynamo radius. These equations only consider the dipole portion of the field, which is assumed to be the dominant component.

These equations should be seen as rough estimates. Following Christensen et al. (2009), we assume that the magnetic field is generated by a dynamo from the release of interior heat (rather than, e.g., rotation). If this is not the case, then magnetic fields are likely to be weaker; however, observational evidence thus far points toward the strong magnetic field case (Cauley et al. 2019). Furthermore, we are applying these relations to lower-mass planets (i.e., hot Saturns) than either Christensen et al. (2009) or Yadav & Thorngren (2017) were originally considering. We expect this is still reasonable because the intrinsic temperatures generating the dynamo are comparable, the conductive liquid-metallic region still extends to most of all our planets' radii, and lastly, since we have used modeled dynamo depths rather than the existing scaling relation from Reiners & Christensen (2010).

For our most massive exo-Io candidate host HD 189733b, $M_P = 1.16\ M_J$, we find $B_{\rm dipole}^{\rm polar} = 58$ G. This translates into a maximum cyclotron frequency of 162 MHz for HD 189733b. For WASP-49b (M_P=0.38 M_J) we find $B_{\rm dipole}^{\rm polar} = 85$ G, and for HAT-P-12b (M_P=0.21 M_J) we find $B_{\rm dipole}^{\rm polar} = 13$ G. These values correspond to a maximum cyclotron frequency of 238 MHz for WASP-49 b and 36.4 MHz for HAT-P-12b. Hence more observations at lower frequencies are required to comment on the ability and presence of an exo-Io to drive ECMI emission at these systems.

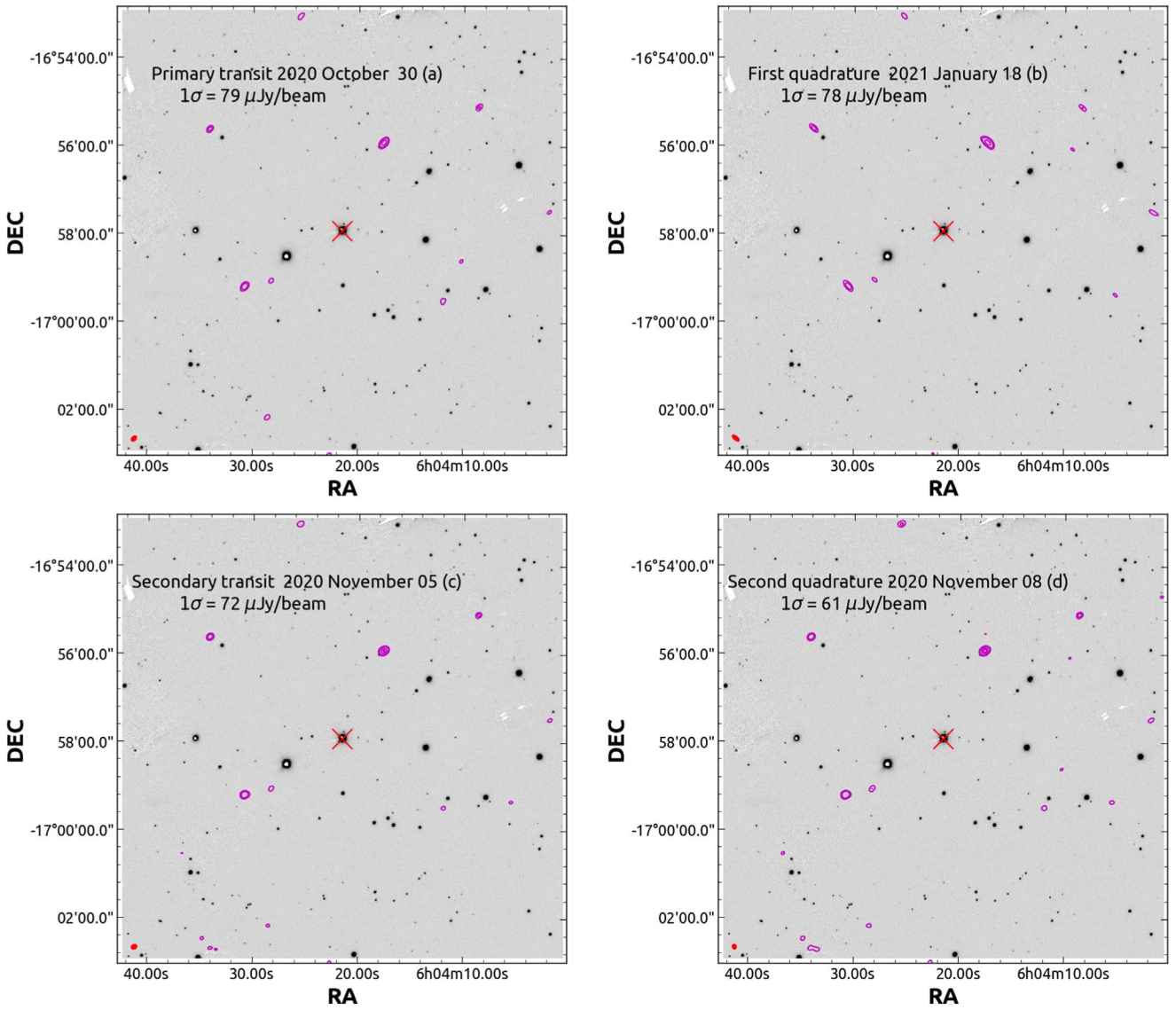

Figure 1. The uGMRT image (magenta contours) of the WASP-49 field at 400 MHz for each of the individual nights of observation overlaid on the PANSTARR g band image. The red cross marks the position of the WASP-49. The contours plotted are 5, 10, 30, and 50 × σ. The beam is shown as a red ellipse at the bottom-left corner.

5.3. Time Variable and Beamed Emission

Radio emissions from planets in our solar system are highly time variable (Zarka et al. 2004). The decameter emission from Jupiter due to the interaction with Io is highly modulated at scales of milliseconds to days (e.g., Zarka et al. 1996; Ryabov et al. 2014). The radio emission from the exomoon interaction could also be a time variable similar to the variability seen in the Jupiter-Io emission. Furthermore, the emission due to the interaction between Io and Jupiter is also highly beamed (e.g., Queinnec & Zarka 1998; Zarka et al. 2004; Ray & Hess 2008; Lamy et al. 2022). Similar beaming is expected from exomoon–exoplanet interactions. Long-term monitoring of these systems (WASP-49, HAT-P 12, and HD189733) would be required to rule out the variable or beamed nature of emission. The nondetection could be explained by Earth not being in the cone of emission at the time of observation.

6. Summary

We present the first dedicated search for radio emission at candidate exoplanet-exomoon systems. We analyzed uGMRT/GMRT observations for three systems, WASP-49, HAT-P 12, and HD 189733. We observed WASP-49 in band 3 (300–550 MHz) of uGMRT. We observed the first and second quadrature as well as the primary and secondary transit of the system in order to search for radio emission and its variability from the system. We do not detect any radio emission from the system but place a strong 3σ upper limit of 0.18 mJy beam^{-1} at 400 MHz. We analyzed archival legacy GMRT data for HAT-P 12 and HD 189733. However, no radio emission was detected from both systems. The HAT-P 12 system was observed at 150 MHz and 325 MHz. At 150 MHz, we obtain a 3σ upper limit of 1.6 mJy beam^{-1} from the HAT-P 12 field; this is one of the deepest images at 150 MHz using GMRT. A much deeper 3σ upper limit of 0.21 mJy beam^{-1} was reached at 325 MHz for this system. We further analyzed legacy GMRT observations of the HD 189733 field at 325 MHz. The 3σ upper limit of 0.36

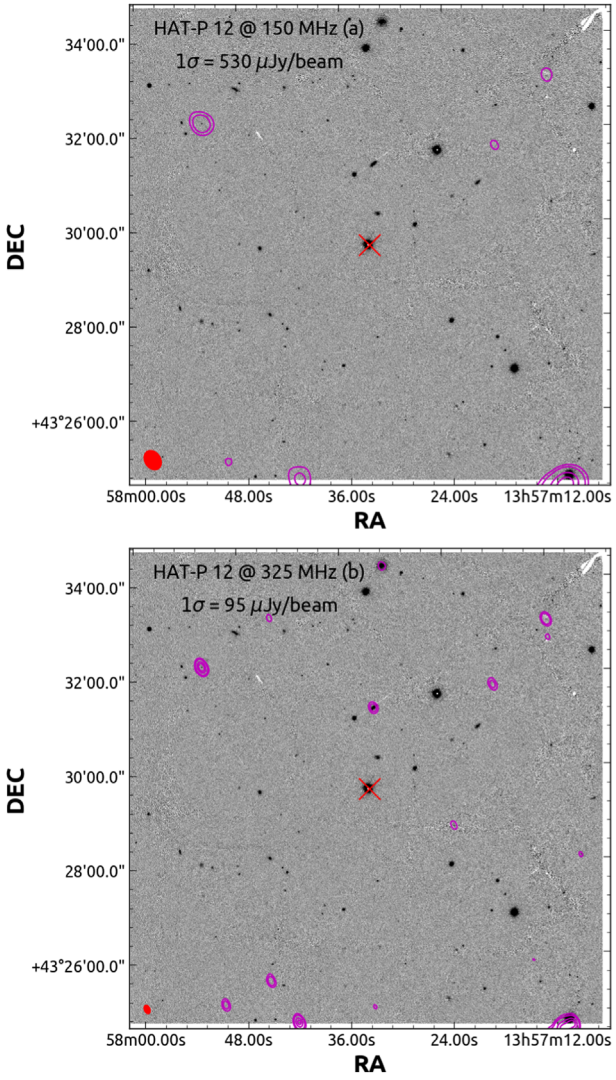

Figure 2. The GMRT image (magenta contours) of the HAT-P 12 field at (a) 150 MHz and (b) 325 MHz overlaid on PANSTARR g band image. The red cross marks the position of the HAT-P 12. The contours plotted are 5, 10, 30, and 50 × σ. The beam is shown as a red ellipse at the bottom-left corner.

mJy beam^{-1} at 325 MHz is 222 times deeper than the previous observation from Smith et al. (2009).

If an exomoon is present in one of these systems, we detect no radio emission due to time variables and beamed emission, overestimation of the cyclotron frequency, or overestimation of the flux density. The search for radio emission due to planet–moon interaction is an emerging field, and more observations at a lower frequency using LOFAR and GMRT band 2 (120–250 MHz) are perhaps required to detect/rule out the presence of exomoons. Indeed, based on the B-field strengths derived here for hot Saturn hosts (Yadav & Thorngren 2017), the majority of exo-Io hosts from Oza et al. (2019) would benefit from searches at lower frequencies. The possibility of evaporating exomoons continues to be tantalizing; however, limited by the characterization of extrasolar gas giant magnetospheres and their interaction with their host stars.

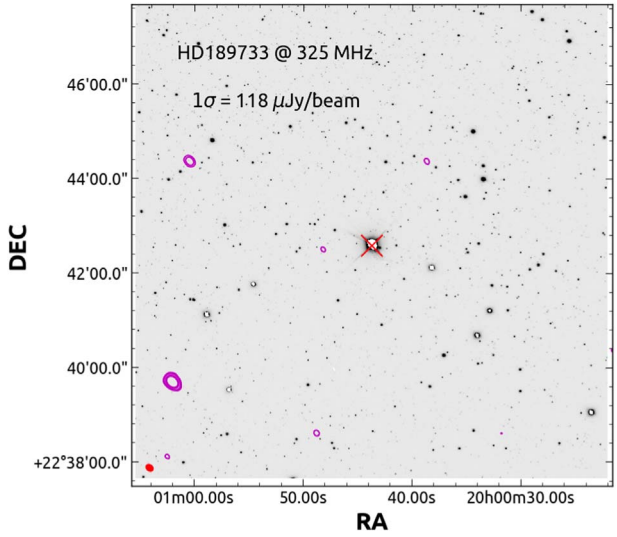

Figure 3. The GMRT image (magenta contours) of the HD 189733 field at 325 MHz images overlaid on the PANSTARR g band image. The red cross marks the position of the HD 189733. The contours plotted are 5, 10, 30, and 50 × σ. The beam is shown as a red ellipse at the bottom-left corner.

This work is based on observations made with the Giant Metrewave Radio Telescope, which is operated by the National Centre for Radio Astrophysics of the Tata Institute of Fundamental Research and is located at Khodad, Maharashtra, India. We thank the GMRT staff for efficient support to these observations. We acknowledge support of the Department of Atomic Energy, Government of India, under Project Identification No. RTI4002. Part of this work was conducted at the Jet Propulsion Laboratory, California Institute of Technology, under contract with NASA. K.H. is supported by the European Research Council via Consolidator Grant ERC-2017-CoG-771620-EXOKLEIN. K.H. is supported by the European Research Council via Consolidator Grant ERC-2017-CoG-771620-EXOKLEIN (awarded to Kevin Heng).

ORCID iDs

Mayank Narang https://orcid.org/0000-0002-0554-1151
Apurva V. Oza https://orcid.org/0000-0002-1655-0715
Kaustubh Hakim https://orcid.org/0000-0003-4815-2874
P. Manoj https://orcid.org/0000-0002-3530-304X
Ravinder K. Banyal https://orcid.org/0000-0003-0799-969X
Daniel P. Thorngren https://orcid.org/0000-0002-5113-8558

References

Addison, B., Wright, D. J., Wittenmyer, R. A., et al. 2019, PASP, 131, 115003
Bailer-Jones, C. A. L., Rybizki, J., Fouesneau, M., et al. 2021, AJ, 161, 147
Belcher, John W. 1987, Sci, 238, 170
Bigg, E. K. 1964, Natur, 203, 1008
Callingham, J. R., Vedantham, H. K., Shimwell, T. W., et al. 2021, NatAs, 5, 1233
Cassidy, T. A., Mendez, R., Arras, P., et al. 2009, ApJ, 704, 1341
Cauley, P. W., Shkolnik, E. L., Llama, J., & Lanza, A. F. 2019, NatAs, 3, 1128
Chabrier, G., Mazevet, S., & Soubiran, F. 2019, ApJ, 872, 51
Christensen, U. R., Holzwarth, V., & Reiners, A. 2009, Natur, 457, 167
Crary, F. J. 1997, JGR, 102, 37
Dwivedi, N. K., Khodachenko, M. L., Shaikhislamov, I. F., et al. 2019, MNRAS, 487, 4208
Gebek, Andrea, & Oza, Apurva V 2020, MNRAS, 497, 5271
Hallinan, G., Sirothia, S. K., Antonova, A., et al. 2013, ApJ, 762, 34
Hartman, J. D., Bakos, G. Á., Torres, G., et al. 2009, ApJ, 706, 785
Heller, R., Rodenbeck, K., & Bruno, G. 2019, A&A, 624, A95

Intema, H. T. 2014, in ASI Conf. Ser. 13, The Metrewavelength Sky, ed. J. N. Chengalur & Y. Gupta (Gujarat: ASI), 469
Kale, Ruta, & Ishwara-Chandra, C. H. 2021, ExA, 51, 95
Kreidberg, L., Luger, R., & Bedell, M. 2019, ApJL, 877, L15
Lamy, L., Colomban, L., Zarka, P., et al. 2022, JGRA, 127, e30160
Lazio, T. J., Farrell, W. M., Dietrick, J., et al. 2004, ApJ, 612, 511
Lecavelier Des Etangs, A., Sirothia, S. K., & Gopal-Krishna 2009, A&A, 500, L51
Lecavelier Des Etangs, A., Sirothia, S. K., & Gopal-Krishna 2011, A&A, 533, A50
Lecavelier Des Etangs, A., Sirothia, S. K., & Gopal-Krishna 2013, A&A, 552, A65
Lendl, M., Anderson, D. R., Collier-Cameron, A., et al. 2012, A&A, 544, A72
Narang, M., Manoj, P., & Ishwara Chandra, C. H. 2021a, RNAAS, 5, 158
Narang, M. 2022, MNRAS, 515, 2015
Narang, M., Manoj, P., Ishwara-Chandra, C. H., et al. 2021b, MNRAS, 500, 4818
Neubauer, F. M. 1980, JGR, 85, 1171
O'Gorman, E., Coughlan, C. P., Vlemmings, W., et al. 2018, A&A, 612, A52
Oza, A. V., Johnson, R. E., Lellouch, E., et al. 2019, ApJ, 885, 168
Pérez-Torres, M., Gómez, J. F., Ortiz, J. L., et al. 2021, A&A, 645, A77
Queinnec, J., & Zarka, P. 1998, JGR, 103, 26649
Ray, L. C., & Hess, S. 2008, JGRA, 113, A11218
Reiners, A., & Christensen, U. R. 2010, A&A, 522, A13
Ryabov, V. B., Zarka, P., Hess, S., et al. 2014, A&A, 568, A53
Saur, J., Neubauer, F. M., Connerney, J. E. P., et al. 2004, Jupiter. The Planet, Satellites and Magnetosphere, Vol. 537 (Cambridge: Cambridge Univ. Press)
Smith, A. M. S., Cameron, A. Collier, Greaves, J., et al. 2009, MNRAS, 395, 335
Su, Y.-J. 2009, IAU Symp. 259, Cosmic Magnetic Fields: From Planets, to Stars and Galaxies (Cambridge: Cambridge Univ. Press), 271
Teachey, A., & Kipping, D. M. 2018, SciA, 4, eaav1784
Thorngren, D. P., & Fortney, J. J. 2018, AJ, 155, 214
Turner, J. D., Zarka, P., Grießmeier, J.-M., et al. 2021, A&A, 645, A59
Vedantham, H. K., Callingham, J. R., Shimwell, T. W., et al. 2020, NatAs, 4, 577
Viswanath, G., Narang, M., Manoj, P., et al. 2020, AJ, 159, 194
Wu, C. S., & Lee, L. C. 1979, ApJ, 230, 621
Wyttenbach, A., Ehrenreich, D., Lovis, C., et al. 2015, A&A, 577, A62
Wyttenbach, A., Lovis, C., Ehrenreich, D., et al. 2017, A&A, 602, A36
Yadav, R. K., & Thorngren, D. P. 2017, ApJL, 849, L12
Zarka, P., Cecconi, B., & Kurth, W. S. 2004, JGRA, 109, A09S15
Zarka, P., Farges, T., Ryabov, B. P., et al. 1996, GeoRL, 23, 125